7378 *Macromolecules* **2010**, *43*, 7378–7385
DOI: 10.1021/ma101142z

Macromolecules
ARTICLE

Dynamics of Semiflexible Dendrimers in Dilute Solutions

Amit Kumar and Parbati Biswas*

Department of Chemistry, University of Delhi, Delhi-110007, India

Received May 27, 2010; Revised Manuscript Received July 12, 2010

ABSTRACT: The dilute solution dynamic properties of dendrimers are theoretically studied in the framework of an optimized Rouse−Zimm approach. Semiflexibility is implemented by modeling topological restrictions on the directions and orientations of the respective bond vectors. This accounts for the neglect of excluded volume interactions in the limit of short spacers. The transport properties, particularly, the behavior of intrinsic viscosity and translational diffusion coefficient are analyzed as functions of flexibility and dendrimer generational growth. The intrinsic viscosity reveals a characteristic maxima, as is experimentally observed in some cases. The value and position of the maxima varies with the topology of the molecule and is mainly dictated by the longest relaxation times. The diffusion coefficient shows a steady decrease for all topologically different conformations up to the fourth generation. The inclusion of hydrodynamic interactions accelerates the dynamics of all semiflexible dendrimer models by decreasing the respective range of intrinsic viscosity and diffusion coefficient values. The structural differences between the different conformations are manifest in the subsequent generations. These topologically dependent flexibility parameters provide suitable approximations to explore the intramolecular dynamics of real dendrimers.

I. Introduction

The design and synthesis of highly branched cascade molecules over the last two decades[1−3] have witnessed a corresponding development in understanding their solution and bulk behavior.[2,4] Compared to the linear polymers of the same molecular mass, dendrimers are highly soluble with decreased melt viscosity and low crystallinity due to interchain entanglements arising from their symmetric branching pattern. From a topological viewpoint, dendrimers may be looked upon as a sequence of concentric shells, each representing monomers of a given generation, growing outward from a central core. The number of monomers increases in a geometric progression for each added shell, resulting in extremely crowded sterically congested peripheries. However the present day picture of dendrimers reveal an open structure[5,6] with a dense core and backfolding branches; thus even a single dendrimer is densely packed within itself.

The dynamic properties of such highly branched macromolecules are complex function of the effects of the branching topology and generational growth and may be determined by different experimental techniques.[7,8] Theoretical approaches to estimate the transport properties are mainly within the framework of optimized Rouse−Zimm models treating the dendrimer in the θ state.[9−11] These calculations are therefore valid in the limit of long spacers for which the dendrimer solution is considered relatively dilute and the concept of the θ state is valid. Some of the recently synthesized dendrimers with relatively short spacers are expected to have strong excluded volume interactions. For such systems, the θ state models are not valid and different types of calculations with excluded volume and hydrodynamic interactions have been attempted[12] which are fairly tedious and time-consuming. Molecular dynamics simulations have also been performed for PAMAM (polyamidoamine) and PPI (polypropyleneimine) dendrimers[13] even though these atomistic models are demanding from the point of view of computation.

*To whom correspondence should be addressed. E-mail: pbiswas@chemistry.du.ac.in.

The intrinsic viscosity of dendrimers present an interesting feature when its variation with the molecular weight is observed experimentally. While the intrinsic viscosity for linear and star polymers increases monotonically with the molecular weight, dendrimers display a maximum in the intrinsic viscosity around fourth to sixth generation.[8] Different calculations based on the variational approach of Fixman by Mansfield and Klushin,[14] hydrodynamic tensor approach of Aerts,[15] radius of gyration by Widmann and Davies[16] and the Brownian dynamics simulations by Adolf et al.[17] also yield the maxima. However, Cai and Chen found a more accurate variant[18] of the Mansfield Klushin theory that does not yield the observed maxima including the long-range excluded volume interactions. Monte Carlo simulation methods[19] using coarse grained idealizations of dendrimers depict a pronounced variation of the viscosity maximum with some of the structural parameters that cannot be captured with simpler models. Few studies to determine the self-diffusion of dendrimers in different concentration regimes have been also reported.[20] However, it is difficult to measure the long-time diffusion coefficient in the semidilute/concentrated regime due to slow diffusion.[20]

In the present paper, the intrinsic viscosity and self-diffusion coefficient of semiflexible dendrimers are evaluated within the optimized Rouse−Zimm approach. Introducing semiflexibility may partially account for the neglect of the excluded volume interactions, especially for short spacers. Hydrodynamic interactions are included via the preaveraged Oseen tensor method which follows a simple r^{-1} screening behavior. Stiffness is implemented in linear chains by orienting the consecutive bond vectors by fixing the average value of the angle between them. This idea is extended to the branched molecules by modeling appropriate restrictions on the respective bond vectors.[21−24] Here we model the restrictions on the respective bond orientations by normalized spherical harmonics $Y_l^m(\theta, \phi)$ such that Y_l^{-m} is equal to the complex conjugate of Y_l^m. These models view the dendrimers as discrete semiflexible polymers and differs from continuum chain models like the wormlike-chain (WLC).[25−27] The choice of the

 Published on Web 07/30/2010

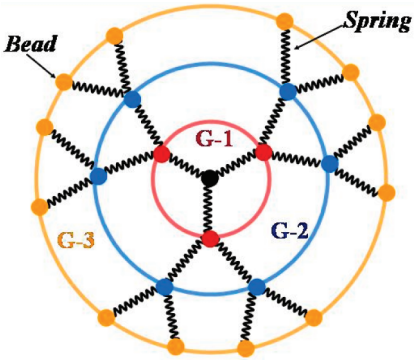

Figure 1. Schematic diagram of a third generation bead−spring model of dendrimer. The circles represent hard beads (monomers), and the springs represent the bond between two monomers.

model leads to the matrix form of the Langevin equation that may be solved in terms of eigenvectors and eigenvalues, some of which may be determined precisely via the iterative procedure.[12]

The paper is organized as follows: In section II, we outline the discrete Rouse−Zimm model for Gaussian chains and introduce semiflexibility and hydrodynamic interactions through adequate approximations. In section III, the transport properties of dendrimers, i.e., intrinsic viscosity and diffusion coefficient, are presented, discussed and their underlying connection with its topology is analyzed. Section IV concludes with the summary of the results.

II. Theory

The structure of dendrimers is schematically represented by a simple bead−spring model Figure 1, in which beads represent monomers and springs indicate the bonds between two monomers. In Figure 1 we depict a dendrimer with $f = 3$ grown up to $g = 3$. There are N beads having identical translational friction coefficients, ζ, connected by $N - 1$ virtual bonds of mean square length l^2. The configuration of such a macromolecule is given by the set of N position vectors, $\boldsymbol{R}_i(t)$, where $\boldsymbol{R}_i(t) = (\boldsymbol{R}_{xi}(t), \boldsymbol{R}_{yi}(t), \boldsymbol{R}_{zi}(t))$ is the position vector of the i-th bead at time t. In the Rouse−Zimm approach, the chain dynamics is governed by the Langevin equation for the bead coordinates $R_i(t)$:

$$\zeta\frac{\partial \boldsymbol{R}_i(t)}{\partial t} + K\sum_{j=1}^{N}[\boldsymbol{H}\cdot\boldsymbol{A}]_{ij}\boldsymbol{R}_j(t) = f_i(t) \tag{1}$$

In eq 1, all bonds are considered equal with the spring constant $K = 3k_BT/l^2$. The first term represents the friction force with the friction coefficient ζ. The second term is the intramolecular interaction potential, which accounts for only the harmonic contribution between monomers directly bound to each other and the hydrodynamic interactions mediated by the solvent. $f_i(t)$ is the stochastic Gaussian force acting on the i-th monomer, with zero mean $\langle f_i(t)\rangle = 0$ and $\langle f_{\alpha i}(t) f_{\beta i}(t')\rangle = 2k_BT\zeta[\boldsymbol{H}^{-1}]_{ij}\delta_{\alpha\beta}\delta(t-t')$ (α and β denote the x, y, and z directions). Where $[\boldsymbol{H}^{-1}]$ is the inverse of matrix to $[\boldsymbol{H}]$. The $N \times N$ matrix $[\boldsymbol{A}] = (A_{ij})$ is the Rouse connectivity matrix or the structure matrix. The elements of this symmetric matrix $[\boldsymbol{A}]$ may be easily calculated; its diagonal element A_{ii} equals the number of bonds emanating from the ith bead, and its off-diagonal elements A_{ij} are either -1 if i and j are connected by a bond, or 0 otherwise. This matrix is related to the incidence matrix $[\boldsymbol{G}]$ by

$$[\boldsymbol{A}] = [\boldsymbol{G}\cdot\boldsymbol{G}^T] \tag{2}$$

where the elements of the rectangular $N \times (N-1)$ matrix $[\boldsymbol{G}]$ are $G_{ij} = -1$ if the bond vector, $\boldsymbol{l}_j$ starts at bead i, $G_{ij} = +1$ if bond vector $\boldsymbol{l}_j$ points to bead i, and $G_{ij} = 0$ otherwise. $[\boldsymbol{A}] = [\boldsymbol{G}\cdot\boldsymbol{G}^T]$ is the inner product of the rows i and j of $[\boldsymbol{G}]$. If $i \neq j$, then these rows have a nonzero entry in the same column if and only if there is a bond joining the beads i and j. Similarly, $[\boldsymbol{G}\cdot\boldsymbol{G}^T]_{ii}$ is the inner product of the row i with itself. Elements of $[\boldsymbol{G}]$ depend on assignments of bond indices and orientations of the bond vectors.

The presence of the solvent molecules is included in the matrix $[\boldsymbol{H}_{ij}]$, which describes the hydrodynamic interaction (HI) between the i-th and j-th monomers and in a simplified picture involves the preaveraged Oseen tensor[26,28] through

$$\boldsymbol{H}_{ij} = (\delta_{i,j} + \zeta_r\langle l/R_{ij}\rangle(1-\delta_{i,j}))\boldsymbol{I} \equiv H_{ij}\boldsymbol{I} \tag{3}$$

where the matrix $[\boldsymbol{H}_{ij}]$ and the identity matrix $[\boldsymbol{I}]$ are both three-dimensional and $R_{ij} = |\boldsymbol{R}_i - \boldsymbol{R}_j|$ is the mutual separation between the centers of the beads i and j. The reduced monomer friction coefficient $\zeta_r = \zeta/6\pi\eta_s l = a/l$, expresses the strength of the hydrodynamic interactions within the preaveraging approximation which gives the effective monomer hydrodynamic radius in units of l. η_s is the viscosity of the solvent. Assuming Gausssian distribution for the intermonomer distances R_{ij}, we get

$$\langle \boldsymbol{R}_{ij}{}^{-1}\rangle = \left(\frac{6}{\pi\langle \boldsymbol{R}_{ij}{}^2\rangle}\right)^{1/2} \tag{4}$$

This distribution of the intermonomer distances may be justified since the flexibility parameters are small and there is no appreciable changes in the shape of the molecule. The hydrodynamic interaction regime is defined by setting a value of $\zeta_r = 0.25$; this value ensures that the matrix $[\boldsymbol{H}]$ is positive definite and does not show any instabilities related to the appearance of negative unphysical eigenvalues. Such eigenvalues occur when the parameter $\zeta_r = \zeta/6\pi\eta_s l = a/l$ exceeds a critical value ζ_r^*, $\zeta_r \geq \zeta_r^*$, which corresponds to the nonoverlapping condition for the monomers ($a/l \leq 0.5$). For dendrimers, ζ_r^* may be topology dependent; thus we choose ζ_r values well below the respective ζ_r^* values in our subsequent calculations.

Semiflexibility is implemented through the topological restrictions on the direction and orientation of the bonds which are looked upon as rigid rotators. The angle between the bond vectors is denoted by θ while ϕ is the angle between the x-axis and projection of any bond vector in the direction perpendicular to it as shown in Figure 2.

The topological restrictions on the bonds are incorporated in the connectivity matrix $[\boldsymbol{A}]$ in terms of the matrix $[\boldsymbol{U}]$, containing the average scalar product of bond vectors

$$[\boldsymbol{A}] = [\boldsymbol{G}\cdot\boldsymbol{U}\cdot\boldsymbol{G}^T] \tag{5}$$

where $[\boldsymbol{U}]$ is a $(N-1)\times(N-1)$ matrix which defines the correlation between the bond vectors in terms of the generalized potential

$$V_s(\boldsymbol{l}_i) = \frac{K}{2}\sum_{i,j} U_{ij}\boldsymbol{l}_i\cdot\boldsymbol{l}_j \tag{6}$$

Evaluating $\langle \boldsymbol{l}_i\cdot\boldsymbol{l}_j\rangle$ with respect to Boltzmann distribution, assuming the bond vectors to be Gaussian distributed the inverse matrix $[\boldsymbol{U}^{-1}]$ is given by

$$[\boldsymbol{U}^{-1}]_{ij} = \frac{\langle \boldsymbol{l}_i\cdot\boldsymbol{l}_j\rangle}{l^2} \tag{7}$$

Hence determining all $\langle \boldsymbol{l}_i\cdot\boldsymbol{l}_j\rangle$ is sufficient to evaluate $[\boldsymbol{U}]$ through a matrix inversion.

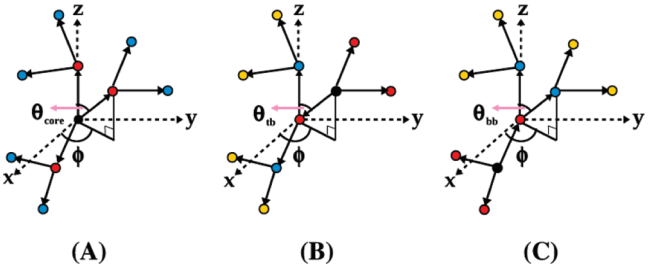

Figure 2. Sketch of bond vector orientaion: (A) θ_{core} is the angle between two bond vectors (red colors) stemming from central core (black colors). (B) θ_{tb} is the angle between the trunk vector pointing to a branching bead and any one branch vector at the branching point. (C) θ_{bb} is the angle between two bond vectors at the branching point. ϕ is the angle between the x-axis and the projection of any bond in the xy plane.

For a spherical polar coordinate system, the restrictions on the respective bond orientations may be modeled by normalized spherical harmonics $Y_l^m(\theta, \phi)$, such that Y_l^{-m} is equal to the complex conjugate of Y_l^m. The choice of this function captures the mutual correlations between consecutive bonds, influenced by the direction of the neighboring bonds in the same or different generations. To a first approximation, this correlation may be modeled by restricting the angle between the bond vectors, θ, to certain values.[22,25] However for real dendrimers hindrances to free rotation extend the range of this correlation between different bond directions. This interdependence of bond directions necessitates the specification of the spatial orientation of the bonds, measured by the bond orientation angle ϕ (refer to Figure 2). For an asymmetric rotational potential, the average scalar product of adjacent bond vectors $\langle \boldsymbol{l}_i \cdot \boldsymbol{l}_j \rangle$ may be defined as;

$$\langle \boldsymbol{l}_i \cdot \boldsymbol{l}_j \rangle = \pm l^2 Y_l^m(\theta, \phi) \tag{8}$$

The bonds are assumed to be directed such that the "+" sign denotes head to tail arrangement while the the "−" sign holds true for other cases. For nonadjacent bonds i and k, the shortest topological distance connecting i and k is chosen.

$$\langle \boldsymbol{l}_i \cdot \boldsymbol{l}_k \rangle = \langle \boldsymbol{l}_i \cdot \boldsymbol{l}_{j_1} \rangle \cdot \langle \boldsymbol{l}_{j_1} \cdot \boldsymbol{l}_{j_2} \rangle \cdots \langle \boldsymbol{l}_{j_n} \cdot \boldsymbol{l}_k \rangle l^{-2n} \tag{9}$$

where $(j_1, j_2, ..., j_n)$ is the unique shortest path connecting i-th and k-th bond vectors. For the zeroth order spherical harmonics i.e., $l = 0$, the bond vectors are spherically symmetric. The angular dependence of the bond vectors is taken into account for the values $l = 1, m = 0$ and $l = 1, m = \pm 1$ by Y_1^0, Y_1^1 and Y_1^{-1} respectively.

$$Y_1^0(\theta, \phi) = \sqrt{\frac{3}{4\pi}} \cos\theta \tag{10}$$

$$Y_1^1(\theta, \phi) = \sqrt{\frac{3}{8\pi}} \sin\theta \exp(i\phi) \tag{11}$$

and

$$Y_1^{-1}(\theta, \phi) = \sqrt{\frac{3}{8\pi}} \sin\theta \exp(-i\phi) \tag{12}$$

For higher order spherical harmonics like $l = 2$, $l = 3$, etc., the inclusion of the hydrodynamic interactions renders the matrix $[\boldsymbol{H} \cdot \boldsymbol{A}]$ unstable which is revealed in the appearance of negative unphysical eigenvalues for generations greater than four.

From eqs 11, 12 any linear combination of Y_1^1 and Y_1^{-1} also represents the direction and orientation of the bond vectors. The normalized linear combination may be expressed as

$$Y_+(\theta, \phi) = \sqrt{\frac{3}{4\pi}} \sin\theta \cos\phi \tag{13}$$

Table 1. Combination of Different Kinds of sin (θ_k) and cos (ϕ) = cos 30° for Semiflexible Dendrimer ($f = 3$, $m = 2$) Using the Spherical Harmonic Approach

models	cos (ϕ) sin θ_{core}	cos (ϕ) sin θ_{tb}	cos (ϕ) sin θ_{bb}
CSM1[a]	$\sqrt{2/3}$	1/2	$\sqrt{15}/6$
CSM2[a]	$\sqrt{2/3}$	1/2	3/4
CSM3[a]	$\sqrt{2/3}$	$\sqrt{2/3}$	$2\sqrt{15}/9$
CSM4[a]	$\sqrt{2/3}$	$\sqrt{2/3}$	$\sqrt{2/3}$

[a] CSMs represent a compressed semiflexible model of dendrimers.

From eqs 8 and 10, the average scalar product of bond vectors may be either defined as

$$\langle \mathbf{l_i} . \mathbf{l_j} \rangle = l^2 \sqrt{\frac{3}{4\pi}} \cos\theta \tag{14}$$

or from eqs 8, 13

$$\frac{\langle \mathbf{l_i} . \mathbf{l_j} \rangle}{l^2} = \sqrt{\frac{3}{4\pi}} \sin\theta \cos\phi \tag{15}$$

The relative orientation of the bond vectors may be tuned by varying the bond projection angle ϕ. A small value of ϕ implies a compressed conformation, while a large value of ϕ implies an expanded conformation. The correlation between the adjacent bonds in a branched macromolecule may be defined by the angles between the respective bond vectors (refer to Figure (2)). Three types of angles between the bond vectors are considered, (i) $\boldsymbol{\theta_{core}}$ between any two bonds in the central core of the dendrimer (ii) $\boldsymbol{\theta_{tb}}$ between any bond vector and the main branch and (iii) $\boldsymbol{\theta_{bb}}$ between any two bond vectors in a given branch originating from the same monomer.[22]

For each combination of θ and ϕ, the corresponding spherical harmonics is obtained which is used to generate the matrix $[\boldsymbol{U}]$ in terms of the equilibrium scalar product of the bond vectors.[23] The combinations of the various θ and ϕ values of the normalized spherical harmonics reprsenting the semiflexible dendrimers are tabulated in Tables 1 and 2.

The solution of this dynamic problem involves solving the Langevin equation Eqn.1 by decoupling into independent normal mode equations by diagonalizing the matrix $[\boldsymbol{H} \cdot \boldsymbol{A}]$. The monomer coordinates are transformed into normal coordinates X by

$$\boldsymbol{R}_j(t) = \sum_{k=1}^{N} Q_{jk} \boldsymbol{X}_k(t) \tag{16}$$

where the matrix $\boldsymbol{Q}$ denotes the matrix of linearly independent normalized eigenvectors of $[\boldsymbol{H} \cdot \boldsymbol{A}]$, defined by the eigenvalue equation

$$[\boldsymbol{H} \cdot \boldsymbol{A}] \cdot \boldsymbol{Q} = \boldsymbol{Q}\Lambda \tag{17}$$

where Λ is a diagonal matrix whose elements are λ_i such that $[\boldsymbol{H} \cdot \boldsymbol{A}]\, \boldsymbol{Q}_i = \lambda_i \boldsymbol{Q}_i$. Then $[\boldsymbol{H} \cdot \boldsymbol{A}] = \boldsymbol{Q}\Lambda\boldsymbol{Q}^{-1}$ holds with $\boldsymbol{Q}^{-1}$ as the inverse of $\boldsymbol{Q}$. The Langevin equation for the generic normal coordinate $\boldsymbol{X}$ is thus

$$\zeta \frac{\partial \mathbf{X}_j(t)}{\partial t} + K\lambda_j \mathbf{X}_j(t) = f_j(t) \tag{18}$$

where the eigenvalues λ_j are obtained from the following relation

$$\langle \mathbf{X}_j(t) . \mathbf{X}_k(t) \rangle = \delta_{jk} \langle \mathbf{X}_j^2(0) \rangle \exp(-tK\lambda_j/\zeta) \tag{19}$$

In the free draining limit, $[\boldsymbol{H}]$ reduces to the identity matrix $[\boldsymbol{I}]$ and therefore eq 18 must be written in terms of the eigenvalues

Table 2. Combination of Different Kinds of sin (θ_k) and cos (ϕ) = cos 150° for Semiflexible Dendrimer ($f = 3$, $m = 2$) Using the Spherical Harmonic Approach

models	cos (ϕ) sin θ_{core}	cos (ϕ) sin θ_{tb}	cos (ϕ) sin θ_{bb}
ESM1[a]	$-\sqrt{2/3}$	$-1/2$	$-\sqrt{15}/6$
ESM2[a]	$-\sqrt{2/3}$	$-1/2$	$-3/4$
ESM3[a]	$-\sqrt{2/3}$	$-\sqrt{2/3}$	$-2\sqrt{15}/9$
ESM4[a]	$-\sqrt{2/3}$	$-\sqrt{2/3}$	$-\sqrt{2/3}$

[a] ESMs represent an expanded semiflexible model of dendrimers.

and eigenvectors of the matrix [A]. The equilibrium matrix [U] also determines the mean square intermonomer distances $\langle R_{ij}^2 \rangle$. An exact analytical expression of $\langle R_{ij}^2 \rangle$ cannot be written because of the topological restrictions on the bond vectors in a complex branched geometry. The distances may be obtained by the diagonalization of matrix [A]

$$\langle R_{ij}^2 \rangle = l^2 \sum_{k=1}^{N-1} \frac{(Q_{ik}^0 - Q_{jk}^0)^2}{\lambda_k^0} \tag{20}$$

where Q^0 and λ^0 are the eigenvectors and eigenvalues of matrix [A] respectively. In the partial draing limit we can write expression for $\langle R_{ij}^2 \rangle$ in terms of eigenvectors and eigenvalues of matrix [$H \cdot A$][10]

$$\langle R_{ij}^2 \rangle = l^2 \sum_{k=1}^{N-1} \frac{(Q_{ik} - Q_{jk})^2}{\lambda_k} \tag{21}$$

where Q and λ are the eigenvectors and eigenvalues of matrix [$H \cdot A$] respectively. For a connected network, the NXN matrix [A] has a nondegenerate zero eigenvalue, since det(A) = 0. For a physically reasonable value of the hydrodynamic interaction parameter, the inverse [H^{-1}] exists and the det(H) $\neq$ 0. Thus, the matrix [$H \cdot A$] has only one zero eigenvalue. Assuming, det($H \cdot A$) = det(H)det(A) = 0, it follows that [$H \cdot A$] has at least one zero eigenvalue, i.e., $\lambda_1 = 0$. The knowledge of the nonzero eigenvalues λ_i and the corresponding eigenvectors is required to determine most of the transport/dynamic properties of the dendrimers like the intrinsic viscosity and diffusion coefficient which play an important role in characterizing macromolecules.

The relative increment of the viscosity of a dilute solution due to the dissolved macromolecule, the intrinsic viscosity [η], is directly proportional to the friction coefficient of the polymer in the solvent. The intrinsic viscosity for all intramolecular modes ($p > 0$) can be expressed in terms of the sum of the relaxation times τ_p as[10,26,28,29]

$$[\eta] = \frac{RT}{2M_b\eta_s} \sum_{p=1}^{N-1} \tau_p \tag{22}$$

where M_b is the bead-mass and τ_p is the relaxation time for the p-th intramolecular mode for any molecule of N normal modes[10,26,28,29]

$$\tau_p = \frac{\zeta}{K\lambda_p} \tag{23}$$

where K, ζ, and λ_p are the spring constant, friction constant and eigenvalues of matrix [$H \cdot A$] respectively. The hydrodynamic radius R_h within the preaveraging approximation is given by the well-known Kirkwood equation[26,28]

$$R_h = N\zeta_r l \left[1 + \frac{\zeta_r}{N} \sum_{i=1}^{N} \sum_{j=1}^{N} (1 - \delta_{ij}) \left\langle \frac{1}{R_{ij}} \right\rangle \right]^{-1} \tag{24}$$

The translational diffusion coefficient D may be calculated from the Stokes−Einstein's equation

$$D = \frac{k_B T}{6\pi\eta_s R_h}$$

which is given by

$$D = \frac{k_B T}{N\zeta} \left[1 + \frac{\zeta_r}{N} \sum_{i=1}^{N} \sum_{j=1}^{N} (1 - \delta_{ij}) \left\langle \frac{1}{R_{ij}} \right\rangle \right] \tag{25}$$

III. Results and Discussion

A. Spectrum and Stability. The results of the previous section require the eigenvalues and the corresponding eigenvectors of the $N \times N$ matrix, [$H \cdot A$], for evaluating the transport properties of semiflexible dendrimers. Usually, [$H \cdot A$] is a dense asymmeteric matrix which may be diagonalized analytically in very special cases. Even for the simplest Rouse model, the sparse matrix [A] can be only diagonalized semianalytically by the recursion scheme.[18] Another work which considers both hydrodynamic and excluded volume interactions, the eigenvalues were computed numerically using QR decomposition.[12] In a related work along the similar lines, the eigenvalues of [$H \cdot A$] were calculated numerically for various adjustable stiffness parameters of the dendrimers.[22] In this work, we consider both semiflexibility and hydrodynamic interactions which makes both matrices, [A] and [H] nontrivial. The N eigenvalues and the corresponding eigenvectors are obtained by directly diagonalizing the matrix [$H \cdot A$] with numerical subroutines.[31] The [$H \cdot A$] matrix is diagonalized for different dendrimeric structures of varying flexibility to obtain the respective set of eigenvalues.

In Figure 3, we compare various eigenvalues of the dendrimers of a specific geometry (with $f = 3$, $n = 1$, and $g = 6$) having varying degrees of flexibility as listed in Table 1,2 with hydrodynamic interactions. In Figure 3, the nonzero eigenvalues of [$H \cdot A$] matrix are plotted in ascending order to depict the relaxation time spectra $1/\lambda_i$ in logarithmic scales. The x-axis shows the number of the eigenvalues, normalized with respect to the total number of monomers N, i.e., i/N. The hydrodynamic interaction parameter (ζ_r) is chosen to be 0.25.[30] The labeled plots (A−D) denote the eigenvalue spectrum for the dendrimers with different flexibility parameters, classified by the enlisted combinations of the angles θ and ϕ. In each case $\lambda_1 = 0$ is an exact eigenvalue which is not shown in the figure. Blue circles indicate the eigenvalues of the semiflexible dendrimers modeled by the spherical harmonics Y_1^0 while the red squares and black triangles depict those with restricted bond orientations, adequately represented by eq 13.

The higher eigenvalues, which correspond to the local modes with slower relaxation, are found to be greater in magnitude for the dendrimers without any restrictions on bond orientations($\phi = 0$), when compared to those having definite bond orientations ($\phi = 30°$,$\phi = 150°$), while the lower eigenvalues are almost similar. Hence the longer relaxation times increase with increasing bond restrictions while the smaller relaxation times remains almost unaffected. Thus, the range of eigenvalues decrease by fixing the bond orientation angle ϕ ($\phi = 30°$, $\phi = 150°$) as compared to $\phi = 0$. No appreciable differences are noted in the lower eigenvalues when the bond orientation angle is either $\phi = 30°$ or $\phi = 150°$, while the higher eigenvalues for $\phi = 30°$ is greater than that for $\phi = 150°$. This also implies

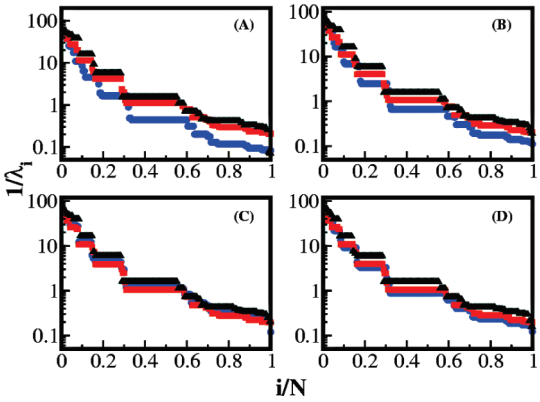

Figure 3. Relaxation spectra ($1/\lambda_i$) for semiflexible dendrimer models with $f = 3$, $n = 1$, and $g = 6$ in partial draining limit ($\zeta_r = 0.25$[30]) vs the normalized mode index (i/N). In the plot blue circles are the eigenvalues of semiflexible dendrimer model with bond orientation angle $\phi = 0$, while those with red squares and black triangles denote the cases with bond orientation angles $\phi = 30°$ and $\phi = 150°$, respectively, as mentioned in Tables 1 and 2. Here eigenvalues λ_i are given in ascending order.

that the longer relaxation times decrease markedly with increasing bond orientation angle while the smaller relaxation times remains almost unchanged.

B. Intrinsic Viscosity. The eigenvalues and normalized eigenvectors of the matrix $[\boldsymbol{H}\cdot\boldsymbol{A}]$ may be used to compute various dynamic properties of dendrimers. Intrinsic viscosity depends only on the eigenvalues, while the translational diffusion coefficient is dependent on both eigenvalues and the normalized eigenvectors of the matrix $[\boldsymbol{H}\cdot\boldsymbol{A}]$. Unlike star or linear polymers, intrinsic viscosity for dendrimers displays a characteristic maximum for a particular generation. This is also experimentally observed in some cases.[7,8] A qualitative explanation of this maxima in intrinsic viscosity of dendrimer can be inferred from the following equation,

$$\lim_{g\to\infty}[\eta] \simeq \lim_{g\to\infty} 1/c^* \Rightarrow \lim_{g\to\infty}[\eta] \Rightarrow V/M \Rightarrow \lim_{g\to\infty} g^3/2^g \longrightarrow 0 \qquad (26)$$

The mass/molecular weight of dendrimers increase exponentially with generation,[7] while its available volume exhibits a cubic power-law behavior. Upto a certain generation, the increase in volume of dendrimers is greater than the increase in its molecular weight, hence $[\eta]$ increases with generation. With increasing generations, the molecular weight increases exponentially and outweighs the increase in volume which results in decreasing $[\eta]$ values after the maxima. The location of this maxima is dependent on the topology of the dendrimer. Equation 22 is used to calculate the intrinsic viscosity of the different representations of semiflexible dendrimers in the following section.

In Figure 4, the intrinsic viscosity of semiflexible dendrimers with $f = 3$ and $n = 1$ are displayed with varying generations. Here, the intrinsic viscosity of semiflexible dendrimers with different bond angle orientations i.e., $\phi = 30°$, $\phi = 150°$, and $\phi = 0$ are plotted and compared with the La Ferla's *TTR* model[22] which is based on a different approach of incorporating stiffness. These plots exhibit similar qualitative behavior; the intrinsic viscosity displays a maximum at a particular generation which may slightly shift for different models. For $\phi = 0$, the behavior of intrinsic viscosity closely resembles La Ferla's *TTR* model spanning the same range, though the numerical magnitude of $[\eta]$ is

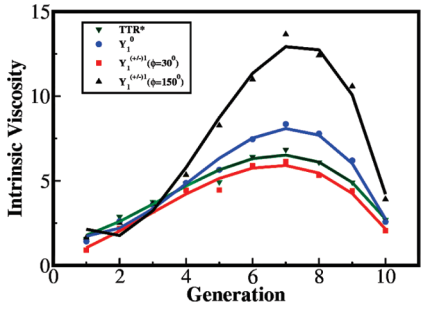

Figure 4. Intrinsic viscosity of semiflexible dendrimer models with bond orientation angles $\phi = 30°$, $\phi = 150°$, and $\phi = 0$ in presence of *HI* as a function of generation and its comparison with La Ferla's *TTR* model[22] (green down triangles). Here red squares, black up-triangles and blue circles represent the semiflexible dendrimer models with different restrictions in bond orientations, i.e., $\phi = 30°$, $\phi = 150°$, $\phi = 0$ respectively. Red, black, blue, and green straight lines are best fit plots.

slightly greater than its corresponding La Ferla value. Compressed semiflexible dendrimers with bond orientation angle $\phi = 30°$ resemble the *TTR* model both in shape and range of $[\eta]$ while the expanded ones with bond orientation angle $\phi = 150°$ exhibits an enhanced range of $[\eta]$ values, especially near the maxima, even though the overall shape is qualitatively similar. Dendrimers with $\phi = 0$ lie between expanded and compressed conformations. From Figure 3 and eq 22 it may be observed that the longer relaxation times for dendrimers with $\phi = 0$ are much lower compared to dendrimers with greater bond orientation restrictions, $\phi = 30°$ and $\phi = 150°$. Hence the magnitude of the maxima is highest for dendrimers having maximum bond orientation restrictions; i.e., $\phi = 150°$.

In Figure 5, the intrinsic viscosity of different semiflexible model dendrimers with different bond orientation angles i.e., $\phi = 30°$ (*CSM*4, refer to Table 1), $\phi = 150°$ (*ESM*4, refer to Table 2) and $\phi = 0$ for $f = 3$ and $n = 1$ are depicted and compared in presence and absence of *HI* respectively. Though the range and shape of the plots are qualitatively similar, the numerical magnitudes of intrinsic viscosity are consistently greater in the absence of *HI* for all semiflexible model dendrimers as compared to their respective values in presence of *HI*. The smaller relaxation times for the semiflexible dendrimers with *HI* are higher than the corresponding ones without *HI*, while the longer relaxation times with *HI* are smaller than the same without *HI*. Hence the range of the intrinsic viscosity is higher for dendrimers without *HI* as compared to those with *HI* for all bond orientation angles i.e., $\phi = 0$, $\phi = 30°$, $\phi = 150°$. Expanded semiflexible dendrimers with bond orientation angle $\phi = 150°$ exhibit an enhanced range of $[\eta]$ values, especially near the maxima as compared to ones with bond orientation angles of $\phi = 0$ and $\phi = 30°$ both in presence and absence of *HI* even though the difference in their relative magnitudes is less in absence of *HI*. This may be due to the fact that the longest relaxation times for semiflexible dendrimers with the bond orientation angle $\phi = 150°$ are higher compared to the ones with the respective angles of $\phi = 0$ and $\phi = 30°$ in the presence and absence of *HI*.

In Figure 6, the intrinsic viscosity of semiflexible model dendrimers are depicted and compared to those having bond orientation angle $\phi = 0$, with hydrodynamic interactions. Different degrees of flexibility are modeled by varying both direction and orientation of bond vectors, i.e., both angles θ and ϕ. The range and shape of the plots corresponding to different semiflexible dendrimers are similar,but the location of the maxima shifts with the change in ϕ. In the labeled plot

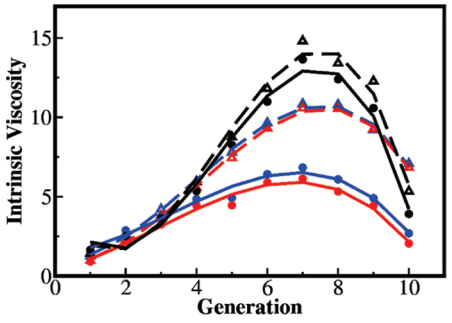

Figure 5. Intrinsic viscosity of semiflexible dendrimer models with bond orientation angles $\phi = 0$, $\phi = 30°$ (*CSM*4 refers to Table 1), $\phi = 150°$ (*ESM*4 refers to Table 2) as a function of generation. Here, circles and up-triangles are for semiflexible dendrimer models in presence and absence of *HI* respectively. In the plot blue, red and black colors represent the semiflexible dendrimer models with different restrictions in bond orientation angle, i.e., $\phi = 0$, $\phi = 30°$, and $\phi = 150°$ respectively. Solid and dotted lines are best fit for the semiflexible dendrimer models in presence and absence of *HI* respectively.

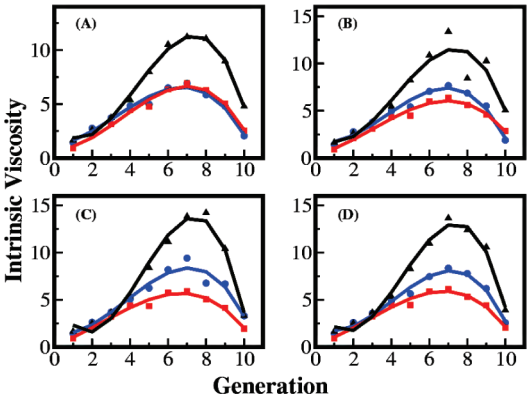

Figure 6. Intrinsic viscosity of semiflexible dendrimer models (refer to Tables 1 and 2) with *HI* as a function of generation and its comparison with model with bond orientation angle $\phi = 0$ (blue circles). Here red squares and black triangles denote semiflexible dendrimer models with the inclusion of restriction in bond orientation $\phi = 30$, 150° as mentioned in Table 1, 2 respectively. Red, black, and blue straight lines are best fit plots.

(*D*), the maximum of intrinsic viscosity occurs in between generations $g = 6$ to $g = 7$ for the compressed dendrimer conformations with $\phi = 0$ and $\phi = 30°$, while for the expanded conformations the maximum is displayed at $g = 8$. The range of intrinsic viscosity for expanded conformations are much higher than the corresponding conformations with $\phi = 0$ and $\phi = 30°$, especially near the maxima.

C. Diffusion Coefficient. Figure 7 depicts the behavior of the diffusion coefficient of various models of semiflexible dendrimers with $f = 3$ and $n = 1$, as a function of different generations of growth. The diffusion coefficient of various semiflexible dendrimer models plotted with specific combination of the angles θ and ϕ are compared to the *TTR* model of La Ferla. The values of the diffusion coefficients for all semiflexible models decrease with the increase in generations. The diffusion coefficient approximately varies as the inverse square root of the number of generations, $D \sim G^{-0.592}$. The values of the diffusion coefficients are almost similar for all semiflexible model dendrimers up to the first four generations. After fourth generation, this value steadily decreases for the expanded conformations($\phi = 150°$) and increases gradually for the respective compressed conformations($\phi = 30°$), compared to the conformations with $\phi = 0$, analogous to the *TTR* model of La Ferla.

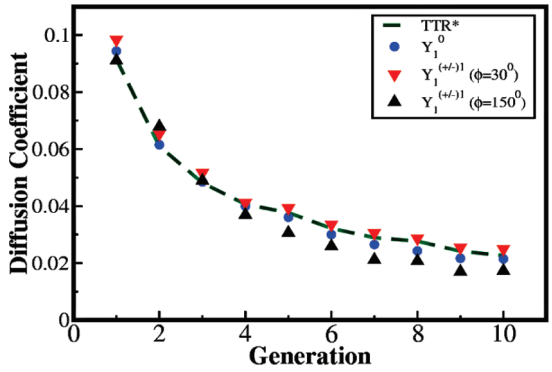

Figure 7. Diffusion coefficient of semiflexible dendrimer models with bond orientation angles $\phi = 30°$, $\phi = 150°$, $\phi = 0$ in presence of *HI* as a function of generation and its comparison with La Ferla's *TTR* module[22] (green dotted line). Here blue circles, red down-triangles and black up-triangles are for semiflexible dendrimer models with the inclusion of restrictions in bond orientations $\phi = 30°$, $\phi = 150°$, $\phi = 0$ respectively.

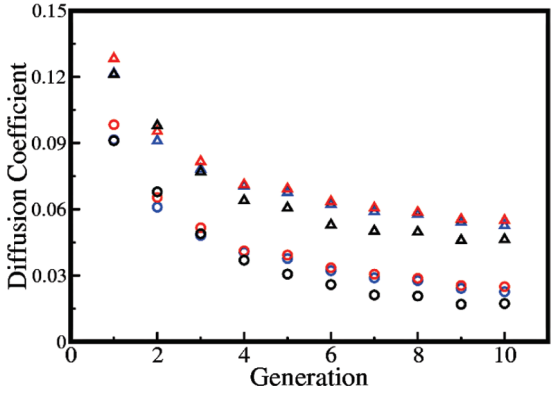

Figure 8. Diffusion coefficient of semiflexible dendrimer models with bond orientation angles $\phi = 0$, $\phi = 30°$ (*CSM*4 in Table 1), $\phi = 150°$ (*ESM*4 in Table 2) in the presence and absence of *HI* as a function of generation. Here, circles and up-triangles are for semiflexible dendrimer models in presence and absence of *HI* respectively. In the plot blue, red and black colors represent the semiflexible dendrimer models with different restrictions in bond orientation angle, i.e., $\phi = 0$, $\phi = 30°$, and $\phi = 150°$, respectively. While solid lines and dotted lines are best fit for the semiflexible dendrimer models in presence and absence of *HI* respectively.

The variation of the diffusion coefficient reveals a good correlation between La Ferla's *TTR* model and the semiflexible model dendrimers with bond orienational angle $\phi = 0$; these values are sandwiched between the compressed and expanded conformations of the semiflexible model dendrimers. The same qualitative trend is reflected in all dendrimers with varying extent of flexibility as shown in Figure9. The expanded conformations exhibit a greater variation in diffusion coefficient values compared to the compressed conformations, as is evident from plots A and B. The compressed conformations resemble those with bond orientational angle $\phi = 0$.

In Figure 8, the diffusion coefficient of semiflexible dendrimers with different bond orientation angles; i.e., $\phi = 30°$ (*CSM*4 refers to Table 1), $\phi = 150°$ (*ESM*4 refers to Table 2), and $\phi = 0$ for $f = 3$ and $n = 1$ are displayed with varying generations. Here, we have compared the diffusion coefficient of semiflexible dendrimers in the presence of *HI* with those of in absence of *HI*. A similar qualitative behavior is observed for the diffusion coefficient of the semiflexible dendrimers with different bond orientation angles, i.e., $\phi = 0$,

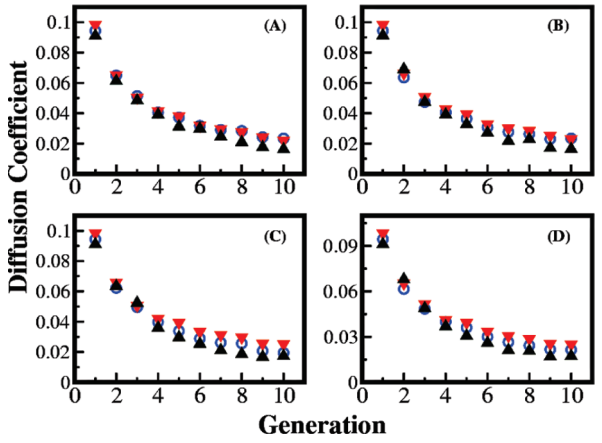

Figure 9. Diffusion coefficient of semiflexible dendrimer models with *HI* as a function of generation and its comparison with the model with bond orientation angle $\phi = 0$ (blue circles). Here red down-triangles and black up-triangles are for semiflexible dendrimer model with the inclusion of restriction in bond orientation $\phi = 30, 150°$ as mentioned in Tables 1 and 2, respectively.

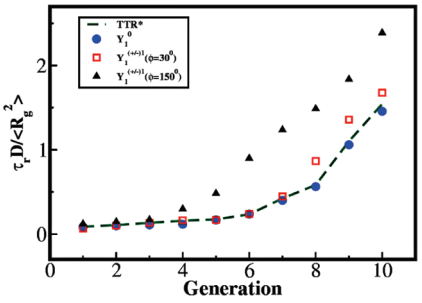

Figure 10. $\tau_r D/\langle R_g^2\rangle$ for semiflexible dendrimer models with bond orientation angles $\phi = 30°$, $\phi = 150°$, $\phi = 0$ in presence of *HI* as a function of generation and its comparison with La Ferla's *TTR* model[22] (green dotted line). Here blue circles, red sqaures and black triangles are for semiflexible dendrimer models *CSM*4, *ESM*4, and semiflexible model with the inclusion of restriction in bond orientation $\phi = 0°$.

$\phi = 30°$, and $\phi = 150°$, respectively, both in the presence and the absence of *HI* (refer to Figure 8). The numerical magnitudes of diffusion coefficient are higher in absence of *HI* than in presence of *HI* for all bond orientation angles.

The translational diffusion coefficient is related to the size of any polymer ($\langle R_g\rangle$) by the equation $\tau_r D \simeq \langle R_g^2\rangle$ where τ_r is the longest relaxation time of any normal mode which is also the time taken by the center of mass of a molecule to diffuse through a distance equal to its average size. For linear and star polymers, $\tau_r D$ varies linearly with the size of the molecule given by $\langle R_g^2\rangle$,[28] and the given ratio is constant. In Figure 10, $\tau_r D/\langle R_g^2\rangle$ is plotted for various values of generation and flexibility parameters. This ratio is constant up to the sixth generation(except for expanded conformations with $\phi = 150°$), after which it shows a steep increase. For expanded conformations with $\phi = 150°$, $\tau_r D$ varies nonlinearly with $\langle R_g^2\rangle$ and the ratio increases sharply after the fourth generation. This deviation at large generations and for expanded conformations points out that the preaveraging approximation fails in this limit and this ratio is no longer constant for highly dense sterically crowded molecules.

IV. Conclusion

In this paper, we theoretically investigate the transport properties of semiflexible dendrimers with appropriate restrictions on their respective bond directions and bond orientations with preaveraged hydrodynamic interactions. Within the optimized Rouse−Zimm framework, the dynamical properties, particularly the intrinsic viscosity and diffusion coefficient are evaluated in dilute solutions. Introducing semiflexibility partly accounts for the neglect of excluded volume interactions, especially in the limit of short spacers. Semiflexibility is implemented through the topological restrictions on both direction and orientation of the respective bonds. The dynamical properties in the present context depend analytically on [*A*], the connectivity matrix, and on [*H*], the hydrodynamic interaction matrix. Intrinsic viscosity depend mainly on the eigenvalues of the matrix [$\boldsymbol{H}\cdot\boldsymbol{A}$] whereas for calculating the diffusion coefficient the normalized eigenvectors are also required. The effect of semiflexibility on the eigenvalue spectrum reveals that the longer relaxation times increase with increasing bond restrictions while the smaller relaxation times remains almost unaffected. Intrinsic viscosity for the semiflexible dendrimers exhibit a maxima between the sixth to seventh generation.

The inclusion of hydrodynamic interactions accelerates the dynamics by decreasing the longest relaxation times and the numerical range of the intrinsic viscosity while the smaller relaxation times are higher. The position of this maxima and the numerical range of the intrinsic viscosity, (especially near the maxima) depends primarily on the lower eigenvalues even though the overall qualitative shape remains same for both expanded and compressed conformations of dendrimers. The diffusion coefficient shows a steady decrease with the increase in generations both in presence and absence of hydrodynamic interactions, with the extent of decrease being sharper in presence of the hydrodynamic interactions. After the fourth generation the expanded conformations show a steady decrease in the diffusion coefficient while the compressed conformations depict an opposite trend. These different topology-dependent flexibility parameters leads to interesting dynamical features which remains to be validated for real dendrimers.

Acknowledgment. The authors gratefully acknowledge the financial assistance from University of Delhi research grant. A.K. gratefully acknowledges UGC-INDIA for providing the Junior Research Fellowship.

References and Notes

(1) Tomalia, D. A.; Baker, H.; Dewald, J.; Hall, M.; Kallos, G.; Martin, S.; Roeck, J.; Ryder, J.; Smith, P. *Polym. J.* **1985**, *17*, 117.
(2) Tomalia, D. A.; Naylor, A. M.; Goddard, W. A., III. *Angew. Chem., Int. Ed. Engl.* **1990**, *29*, 138.
(3) Fréchet, J. M. J.; Hawker, C. J.; Wooley, K. L. *J. Macromol. Sci.—Pure Appl. Chem.* **1994**, *A31*, 1627.
(4) Fréchet, J. M. J. *Science* **1994**, *263*, 1710.
(5) de Gennes, P. G.; Hervet, H. J. *J. Phys.* (*Paris*) **1983**, *44*, L351.
(6) Naylor, A. M.; Goddard, W. A., III; Kiefer, G. E.; Tomalia, D. A. *J. Am. Chem. Soc.* **1989**, *111*, 2339.
(7) Mourey, T. H.; Turner, S. R.; Rubinstein, M.; Fréchet, J. M. J.; Hawker, C. J.; Wooley, K. L. *Macromolecules* **1992**, *25*, 2401.
(8) Fréchet, J. M. J.; Tomalia, D. A. *Dendrimers and other Dendritic polymers*; Wiley: Chichester, England, 2001.
(9) Bixon, M.; Zwanzig, R. *J. Chem. Phys.* **1978**, *68*, 1896.
(10) Perico, A.; Ganazzoli, F.; Allegra, G. *J. Chem. Phys.* **1987**, *87*, 3677.
(11) Gurtovenko, A. A.; Blumen, A. *Adv. Polym. Sci.* **2005**, *182*, 171.
(12) Chen, Z. Y.; Cai, C. *Macromolecules* **1999**, *32*, 5423.
(13) Jana, C.; Jayamurugan, G.; Ganapathy, R.; Maiti, P. K.; Jayaramana, N.; Sood, A. K. *J. Chem. Phys.* **2006**, *124*, 204719.
(14) Mansfield, M. L.; Klushin, L. I. *J. Phys. Chem.* **1992**, *96*, 3994.
(15) Aerts, J. *Comput. Theor. Polym. Sci.* **1998**, *8*, 49.
(16) Widmann, A. H.; Davies, G. R. *Comput. Theor. Polym. Sci.* **1998**, *8*, 191.
(17) Lyulin, A. V.; Davies, G. R.; Adolf, D. B. *Macromolecules* **2000**, *33*, 3294.
(18) Cai, C.; Chen, Z. Y. *Macromolecules* **1997**, *30*, 5104.
(19) Freire, J. J.; Rodriguez, E. *J. Chem. Phys.* **2005**, *123*, 154901.

(20) Rietveld, I. B.; Bedeaux, D. *Macromolecules* **2000**, *33*, 7917.
(21) Guenza, M.; Perico, A. *Macromolecules* **1992**, *25*, 5942.
(22) La Ferla, R. *J. Chem. Phys.* **1997**, *106*, 688.
(23) von Ferber, C.; Blumen, A. *J. Chem. Phys.* **2002**, *116*, 8616.
(24) Dolgushev, M.; Blumen, A. *Macromolecules* **2009**, *42*, 5378.
(25) Flory, P. J. *Statistical Mechanics of Chain molecules*; Interscience Publishers, John Wiley and Sons: New York, 1969.
(26) Yamakawa, H. *Modern Theory of Polymer Solutions*; Harper & Row: New York, 1971.
(27) Yamakawa, H. *Annu. Rev. Phys. Chem.* **1984**, *35*, 23.
(28) Doi, M.; Edwards, S. F. *The Theory of Polymer Dynamics*; Claerndon Press: Oxford, U.K., 1986.
(29) Zimm, B. H. *J. Chem. Phys.* **1956**, *24*, 269.
(30) Biswas, P.; Kant, R.; Blumen, A. *J. Chem. Phys.* **2001**, *114*, 2430.
(31) Press, W. H.; Teukolsky, S. A.; Vetterling, W. T.; Flannery, B. P. *Numerical Recipes in Fortran*, 2nd ed.; Cambridge University Press: Cambridge, U.K., 1992.